ACS APPLIED MATERIALS & INTERFACES

Research Article

www.acsami.org

Zinc–Air Battery: Understanding the Structure and Morphology Changes of Graphene-Supported $CoMn_2O_4$ Bifunctional Catalysts Under Practical Rechargeable Conditions

Moni Prabu,[†] Prakash Ramakrishnan,[†] Hiroki Nara,[‡] Toshiyuki Momma,[‡,§] Tetsuya Osaka,[‡,§] and Sangaraju Shanmugam*[,†]

[†]Department of Energy Systems Engineering, Daegu Gyeongbuk Institute of Science and Technology (DGIST), Daegu 711-873, Republic of Korea

[‡]Faculty of Science and Engineering and [§]Graduate School of Advanced Science and Engineering, Waseda University, 3-4-1 Okubo, Shinjuku-ku, Tokyo 169-8555, Japan

Supporting Information

ABSTRACT: Nitrogen-doped/undoped thermally reduced graphene oxide (N-rGO) decorated with $CoMn_2O_4$ (CMO) nanoparticles were synthesized using a simple one-step hydrothermal method. The activity and stability of this hybrid catalyst were evaluated by preparing air electrodes with both primary and rechargeable zinc–air batteries that consume ambient air. Further, we investigated the relationship between the physical properties and the electrochemical results for hybrid electrodes at various cycles using X-ray diffraction, scanning electron microscopy, galvanodynamic charge–discharging and electrochemical impedance spectroscopy. The structural, morphological and electrocatalytic performances confirm that CMO/N-rGO is a promising material for safe, reliable, and long-lasting air cathodes for both primary and rechargeable zinc–air batteries that consume air under ambient condition.

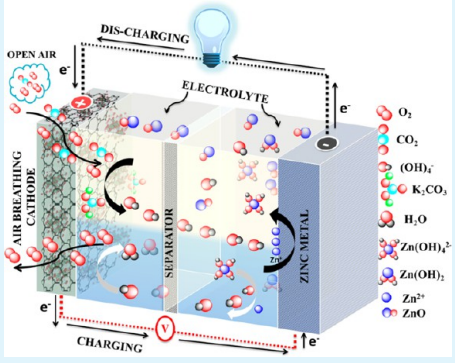

KEYWORDS: *bifunctional catalyst, zinc–air battery, ambient condition, structural stability, surface morphology*

1. INTRODUCTION

Compared with other chemical-based batteries, metal–air batteries, as a result of their high theoretical energy densities, can contribute greatly to address the problems involved in the rapid growth of applications, particularly in the fields of electric and hybrid electric vehicles.[1−4] Among the various metal–air batteries, the zinc–air battery has been considered as an attractive choice because of its unique benefits, such as low cost, safety, and environmental benignity.[1,5−9] Because of the drawbacks accompanying the commercialization of zinc–air batteries, such as the slow kinetics of the oxygen reduction reaction (ORR) and the oxygen evolution reaction (OER), which result in large overpotentials, tremendous interest has been devoted to the development of more highly efficient, alternative novel bifunctional electrocatalysts that are effective for both ORR and OER processes.[7,10−18] Given this background, there has been massive development of new bifunctional air-breathing cathode materials, with promising electrocatalystic activity that could significantly reduce the overpotential and enhance the cyclic stability toward the realization of a rechargeable zinc–-air battery. Chen et al.[19] reported that Co_3O_4 nanowires directly grown on a stainless steel mesh current collector exhibited remarkable rechargeability and stability in a practical zinc–air battery using natural air. Dai et al. investigated a CoO/carbon nanotube hybrid with Ni–Fe-layered double hydroxide electrocatalysis for primary and rechargeable Zn–air batteries.[8] High electrocatalytic activities of hybrid MnO_2/Co_3O_4 nanoparticles have been reported by Liu et al.[6] and Lee et al.[17] reported that a layered perovskite structure can serve as an efficient bifunctional electrocatalyst with improved round-trip efficiency as well as high stability during cycling for a zinc–air battery. Chen et al. showed that a core–corona structured $LaNiO_3$ supporting with nitrogen-doped carbon nanotubes had outstanding ORR and OER activity in rechargeable zinc–air batteries.[14] Recently, we investigated the use of spinel materials like 1D-$NiCo_2O_4$ and $CoMn_2O_4$/N-rGO as bifunctional air electrodes for zinc–air batteries under pure oxygen atmosphere.[10,11]

The complex steps involved in metal–air batteries arise from cathode compartments with bifunctional catalysts; these compartments have to work with a triple phase interface composed of oxygen gas, liquid electrolyte, and solid catalyst. There are several potential problems with these cathode compartment: (i) mechanical breakdown generated on the catalyst from the air–cathode surface caused by oxygen evolution during charging; (ii) atmospheric CO_2 can react with hydroxyl ions to form

Received: May 9, 2014
Accepted: September 5, 2014
Published: September 5, 2014

carbonates; (iii) formation of discharge product ZnO deposit on the surface can lead to severe failure of the air cathode, which will limit the lifetime of a zinc−air battery with a large overpotential.[1] Therefore, it is quite reasonable to understand the structure and morphological changes that occur on a bifunctional air electrode when it is cycled with strong alkaline medium, consuming air under ambient condition. Such evidence is vital to the successful development of practical storage devices.[19−25] Previously, for academic interest, we studied the preliminary electrocatalytic performance of graphene supported $CoMn_2O_4$ (CMO) nanoparticles using pure oxygen atmosphere.[10] From a commercial point of view, this is a very important area of study for the development of zinc−air batteries that operate in ambient air condition instead of utilizing a pure oxygen atmosphere.[26,27] To the best of our knowledge, for the first time, we here correlate the electrode surface chemistry, morphology, and cycling efficiency at various charging−discharging cycles over graphene supported CMO bifunctional catalysts in a rechargeable zinc−air battery under practical conditions.

2. EXPERIMENTAL SECTION

Graphene oxide (GO) was prepared from graphite flakes using a modified Hummers' method.[28] The hybrid materials CMO/rGO, CMO/N-rGO, and CMO were prepared using a one pot hydrothermal method. A typical synthesis of CMO/N-rGO was carried out as follows: 33 mg GO was dispersed in 100 mL of ethanol, followed by the addition of 1.65 mL of 0.2 M cobalt acetate, 3.65 mL of 0.2 M manganese acetate, and 2.08 mL of NH_4OH. The mixture was refluxed at 80 °C for 10 h, transferred to an autoclave, and heated at 150 °C for 3 h. The sample was rinsed with water and ethanol and dried at 70 °C overnight. In contrast, CMO/rGO hybrid was prepared using the same process, but without NH_4OH and CMO nanoparticles prepared without either GO or nitrogen sources.[10,29,30]

The thermal stability of the catalysts was studied using a thermogravimetric analyzer (Rigaku, TG 8120) from 30 to 1000 °C at a heating rate of 10 °C/min in air atmosphere. The structural stability of the cycled electrodes was studied using an X-ray diffractometer (Rigaku) after the cells were dismantled and the air-breathing electrodes were recovered. The morphology of the graphene supported CMO bifunctional catalysts before and after cycling was analyzed using a field emission-scanning electron microscope (FE-SEM, Hitachi). Decoration of CMO nanoparticles on the graphene support was observed using a field emission-transmission electron microscope (FE-TEM, Hitachi). The rechargeability of the zinc−air battery was determined using a split test cell (EQ-STC-MTI-Korea). The electrodes were fabricated with an active material, isopropyl alcohol (IPA), and 5 wt % Nafion ionomer solutions at a weight ratio of 9.4 mg:1 mL:67 μL coated on a gas diffusion layer (SGL, thickness = 0.27 mm). Air electrodes with geometrical area of 2.54 cm^2 were coated with 3 mg of catalyst using an airbrush to achieve a loading of 1.18 mg cm^{-2}. A polished zinc plate was the negative electrode (anode), a Whatman glass microfiber filter membrane was used as a separator, and 6 M KOH was used as the electrolyte. The charge−discharge studies were carried out using a Battery Analyzer (BST8−3); battery cells consumed air under ambient condition. The impedance spectra of the cells were measured at a dc potential of 0.8 V with an ac signal amplitude of 10 mV and a variable frequency range from 10 kHz to 10 mHz. More details of the material preparation and electrode fabrication were presented in our previous studies.[10,11]

3. RESULTS AND DISCUSSION

3.1. Thermal and Morphology Effects. The actual loading of CMO nanoparticles anchored on the surface of rGO was determined by TGA analysis (Figure 1). During a subsequent heat treatment, functional groups of GO were simultaneously

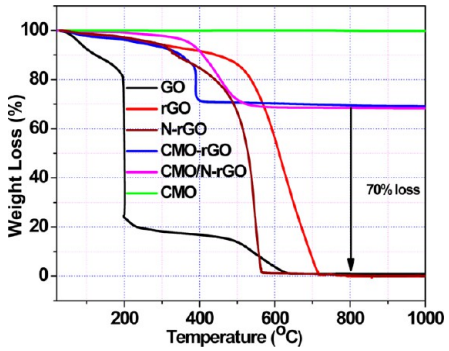

Figure 1. Thermograms of GO, rGO, N-rGO, CMO, CMO/rGO, and CMO/N-rGO with a heating rate of 10 °C/min in air atmosphere.

reduced by Co and Mn metal ions when Co−Mn hydroxide was transformed into $CoMn_2O_4$.[31] Further, residual functional groups of GO were reduced and nitrogen-doped by ammonia, which enhanced the thermal stability of the N-rGO compared with that of the pristine GO sheets (Figure 1). The thermogram shows that the rGO sheets were completely burned off at 800 °C, while CMO is stable throughout the temperature range. The weight loss values at 800 °C, which were found to be 30 and 31%, can be attributed to the support from the hybrids of CMO/rGO and CMO/N-rGO, respectively. On the basis of the TGA weight loss, the mass ratio of CMO/rGO was calculated and found to be 7/3.[15,32]

SEM images of hybrid materials show that spherical CMO nanoparticles with an average diameter of 20 nm are uniformly dispersed on the wrinkled N-rGO sheets, whereas the CMO/rGO hybrid reveals that larger particles with an average diameter of 30 nm are randomly dispersed on and outside of the rGO supports (Figure 2). Without the rGO support, the as-prepared CMO particles (~40 nm) are larger than the hybrids and the particles are highly agglomerated due to lack of a supporting layer to prevent the CMO nanoparticles from aggregation. Figure 3a−f shows the typical TEM and HRTEM images of the as-synthesized hybrid nanoparticles. It can be seen from the TEM image that the GO sheets have been exfoliated and the CMO nanoparticles are well decorated. The HRTEM images of CMO/N-rGO confirms the good crystalline nature, with a nice distribution of CMO nanoparticles on the N-rGO surface.[29,30,33] The inter layer spacings are found to be 0.15, 0.25, and 0.29 nm, corresponding to the (224), (211), and (200) planes of the tetragonal phase CMO nanoparticles (JCPDS card no. 077−0471).[34] Further, from the TEM elemental mapping (Figure 4), we can see the uniform distribution of Co, Mn, O, C, and N elements in the CMO/N-rGO hybrid materials, indicating that the doped nitrogen is uniformly distributed in the rGO.[15] The distribution of nitrogen functional groups was identified from XPS spectrum and it was observed that pyridinic nitrogen group content was predominant (55 wt % of pyridinic nitrogen at 399.1 eV and 15% of quaternary nitrogen at 402.1 eV is usually functioning as electro catalytic active sites than 30 wt % of pyrrolic nitrogen at 400.3 eV).[10,35] The deconvoluted Co 2p XP spectrum exhibits two spin orbit doublets of Co^{2+} and Co^{3+} along with two shakeup satellites peaks (see Figure S2 in the Supporting Information). On the other hand Mn 2p spectrum was fitted with four peaks, indicate the existence of Mn in both Mn^{2+} and Mn^{3+}. The high-resolution XPS spectra of Co 2p, Mn 2p, and O 1s shifted to positive binding energy after doping with

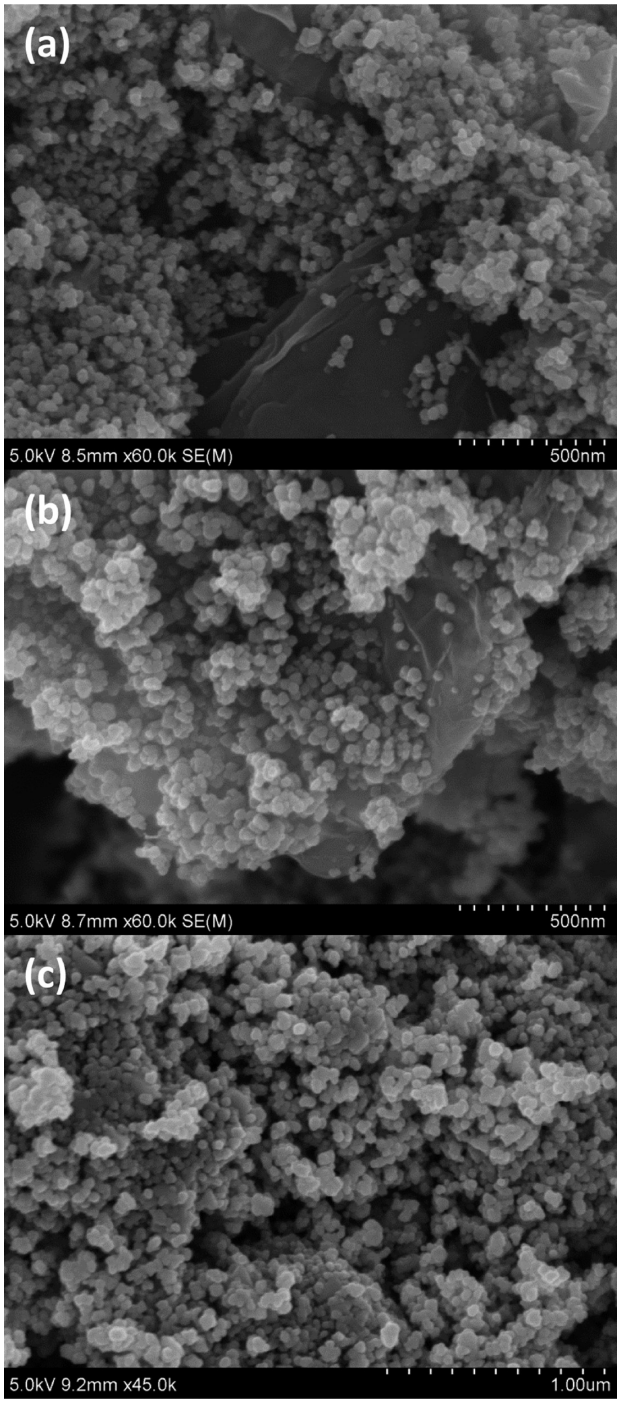

Figure 2. SEM images of (a) CMO/rGO; (b) CMO/N-rGO; and (c) CMO nano particles.

nitrogen in the rGO hybrid, which undoubtedly further confirms the strong interaction between CMO and N-rGO surface (see Figure S2 in the Supporting Information).[10] This feature might be beneficial for enhancing the electrocatalytic behavior, which will be discussed in subsequent sections.

3.2. Primary Zinc–Air Battery. To understand the practical stability of the hybrid catalyst under deep discharging state, we first constructed a primary zinc–air battery and the battery was discharged it at room temperature to a 0.5 V limit with a current density of 20 mA cm^{-2}; the battery consumed air under ambient condition (Figure 5a). Both catalysts

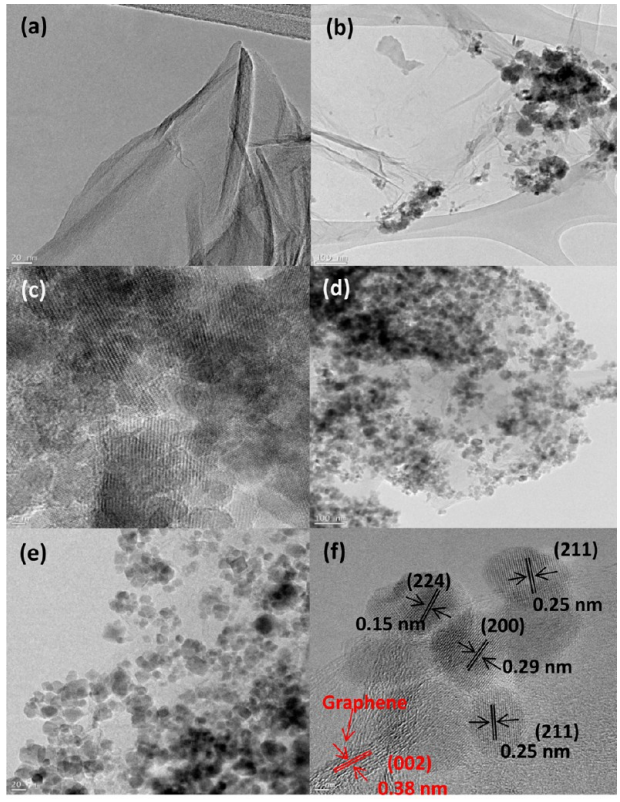

Figure 3. TEM and HRTEM image of (a) GO; (b, c) CMO/rGO; and (d–f) CMO/N-rGO hybrid.

showed open circuit voltage at ca. 1.5 V vs Zn, followed by a well-defined plateau region at ca. 1.15 V over 12 h; this shows the outstanding stability of the hybrid materials toward the oxygen reduction reaction. The overall reduction reaction mechanism in the primary zinc–air battery is

Cathode:

$$O_2 + 2H_2O + 4e^- \rightarrow 4OH^- \quad (E_0 = 0.4V) \tag{1}$$

Anode:

$$Zn \rightarrow Zn^{2+} + 2e^- \tag{2}$$

$$Zn^{2+} + 4OH^- \rightarrow Zn(OH)_4^{2-}(soln) \quad (E_0 = -1.25V) \tag{3}$$

$$Zn(OH)_4^{2-}(soln) \rightarrow ZnO(s) + H_2O + 2OH^- \tag{4}$$

Parasitic anode reaction:

$$Zn + 2H_2O \rightarrow Zn(OH)_2 + H_2\uparrow \tag{5}$$

Parasitic cathode reaction:

$$2KOH + CO_2 \rightarrow K_2CO_3 + H_2O \tag{6}$$

In general, the equilibrium potential of the zinc–air battery should be 1.65 V, but both hybrid electrodes showed a plateau region at ca. 1.15 V; which is due to the sluggish four-electron oxygen reduction reaction, caused by internal, ohmic, and concentration losses.[1] A discharge capacity of 460 mAh g^{-1} was observed for the CMO/rGO hybrid cathode, whereas an improved capacity of 610 mAh g^{-1} was achieved for the CMO/N-rGO hybrid (Figure 5b). The obtained discharge capacity value is comparable to those of primary Zn–air batteries constructed using CoO/N-CNT[8] and one-dimensional

dx.doi.org/10.1021/am5047476 | ACS Appl. Mater. Interfaces 2014, 6, 16545–16555

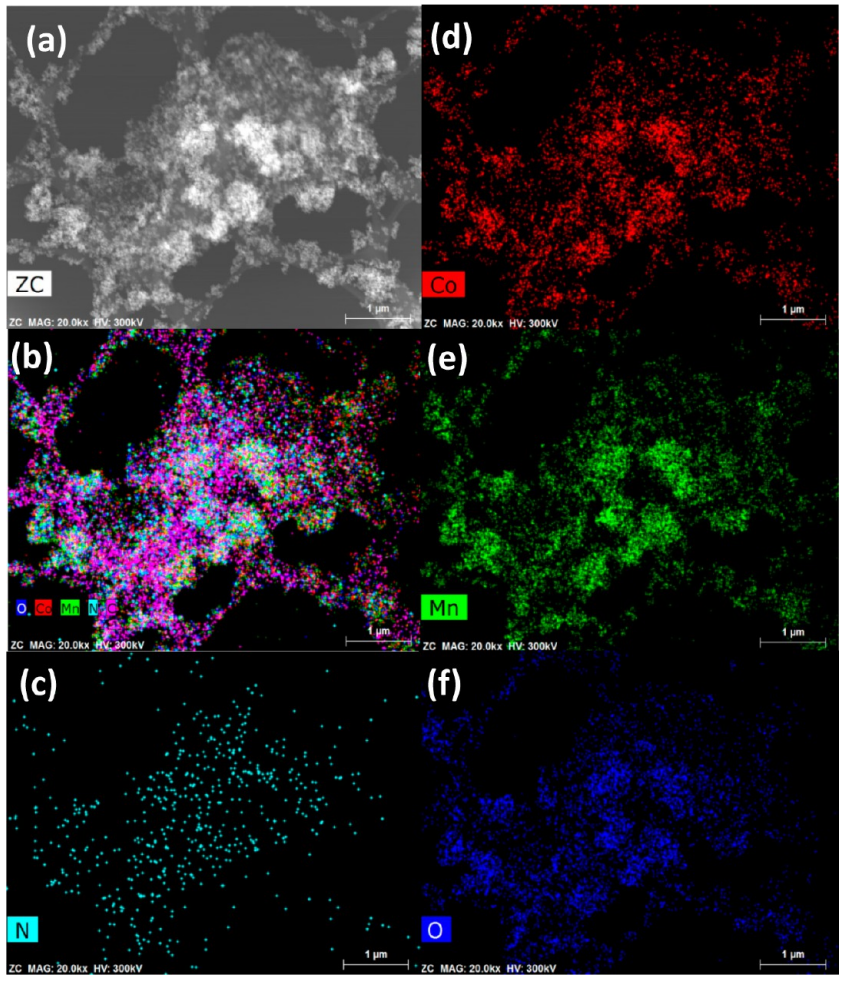

Figure 4. TEM elemental mapping of CMO/N-rGO hybrid: (a) bright-field TEM image; (b) overlay images; (c) N−K edge; (d) Co−K edge; (e) Mn−K edge; and (f) O−K edge.

$NiCo_2O_4$-based[11] cathode materials. From the OCV, plateau region, discharge time, and discharge capacity of CMO/N-rGO has outperformed CMO/rGO as a result of the increase in its electronic conductivity due to N-doping in rGO, which induces extra charge carriers with the positive effect of pyridinic and graphitic-nitrogen and the morphological effect.[18] Furthermore, nitrogen doped on the graphene layer creates graphene edge defects, which will push the edge sites to adsorb more oxygen molecules and enhance the catalytic activity of the zinc−air battery during deep discharging.[36,37]

3.3. Rechargeable Zinc−Air Battery. Our preliminary results show that a strong chemical coupling between CMO nanoparticles anchored on N-rGO support lead to an outstanding bifunctional catalytic activity in alkaline condition compared with a noble metal catalyst (Pt/C) in Zinc-Air battery (ΔE = 0.86 V; 150 mV better than rGO support) and half-cell measurement (ΔE = 0.86 V; 60 mV better than rGO support) systems that consume pure oxygen (Table 1).[10] In this study, we investigate the rechargeability and durability of bifunctional air electrodes that consume air under practical conditions. The zinc−air battery was tested with short (10 min) and long intervals (1and 2 h) cycles, while consuming air under an ambient condition instead of using pure oxygen gas. The charge−discharge (C−D) performances of the hybrids CMO/N-rGO and CMO/rGO over 200 cycles are presented in Figure 6a−c. The possible charging mechanism for the zinc−air battery is explained as

$$Zn(OH)_4^{2-}{}_{(soln)} + 2e^- \rightarrow Zn + 4OH^- \quad (7)$$

$$4OH^- \rightarrow O_2 + 2H_2O + 4e^- \quad (8)$$

During the C−D process, the Zn/Zn^{2+} redox reaction at the anode and the oxygen reduction-evolution reaction on the cathode occur simultaneously. During discharge conditions, zinc metal is oxidized at the anode, while oxygen is reduced to hydroxide ion on the cathode surface via four electron-transfer reaction (calculated using a K−L plot at different potentials as described in our previous report);[10] the hydroxide ion react with Zn^{2+} to form a soluble zincate ($Zn(OH)_4^{2-}$) ion, which is further dehydrated to form ZnO, a white solid product which acts as an insulator, making rechargeability a challenging task (based on eqs 1-4). Simultaneously, a pair of undesired reactions between positive and negative electrode materials occur (eqs 5 and 6): (i) the zinc metal reacts with the alkaline electrolyte (KOH), resulting in the formation of $Zn(OH)_2$ and the generation of hydrogen gas, which causes a gradual corrosion of the zinc metal at anode; and (ii) CO_2 from ambient air reacts with the alkaline electrolyte, which leads to the formation of carbonate (K_2CO_3) deposited on the cathode surface which lowering the performance.[38] In the case of charging, there are various complicated steps involving and difficult reverse process

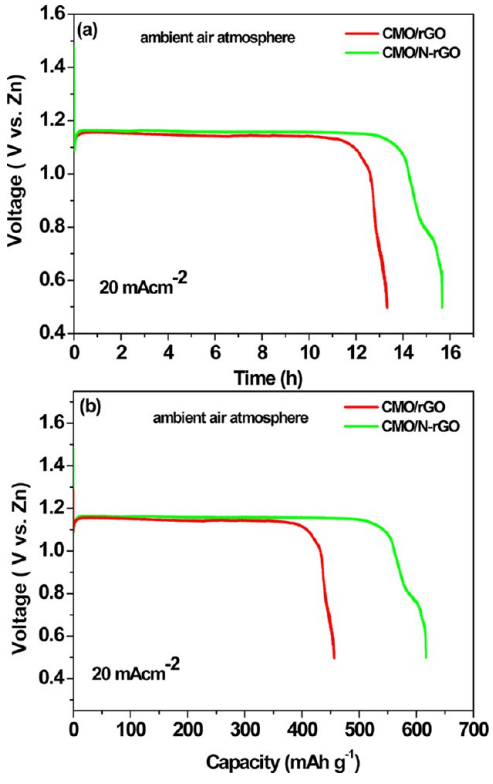

Figure 5. (a) Discharge profiles of CMO/rGO and CMO/N-rGO hybrid consuming air under ambient condition at a current density 20 mA cm^{-2}, deep discharge to a cutoff potential of 0.5 V vs Zn. (b) Specific discharge capacity of CMO/rGO and CMO/N-rGO hybrid.

of the discharging process, with the evolution of oxygen at the air cathode surface (based on eqs 7 and 8).[23,39] Using CMO/N-rGO catalyst, the initial potential gap between the charge and discharge was about 0.7 V; this value slowly increased to 1.06 V after 200 cycles, but, in the case of CMO/rGO, the value increased to 1.23 V from 0.95 V, as shown in Figure 6a, d. From the battery performance, it can be seen that the CMO/N-rGO hybrid shows lower overpotential with minimal fluctuation in the potential gap when compared with those characteristics of the CMO/rGO catalyst. These differences are the result of N-doping on CMO/rGO, which creates more active sites during the cycling than is the case for CMO/rGO materials. In addition, the CMO/N-rGO catalyst showed perfect flat potential curves for both discharge and charge process, whereas CMO/rGO showed an almost flat region within this interval (Figure 6a). In our previous report, we have shown that the charge−discharge property of hybrid catalysts under oxygen environment.[10] So, it would be interesting to compare the overpotential required for charge−discharge process under different atmospheres, from pure oxygen to air under ambient condition.[16] For the CMO/N-rGO catalyst, the potential gap slowly increases from 0.70 to 0.86 V after 100 cycles when pure oxygen is used, whereas in ambient air condition the potential gap increased to 0.93 V from 0.86 V. In the case of CMO/rGO, the potential gap increases from 0.71 to 0.95 V after 100 cycles in pure oxygen, while this value increased to 1.1 V from 1.01 V in ambient air (Figure 6d, Table 1). Consequently, both catalysts showed slightly higher overpotential under ambient air condition than they did in pure oxygen because of the lower O_2 concentration in ambient air and noticeable carbonate formation on the cathode surface.[16] For a better practical understanding, the long-term cyclability (1 and 2 h cycles) of hybrid electrodes was tested and compared with that of electrodes using noble Pt/C catalyst (Figure 6b, c). Both hybrid catalysts show excellent charge−discharge profiles for a given interval of time, whereas the Pt/C catalyst shows a better discharge profile for the initial cycle and significantly worse in charge performance at higher potential, even affecting the consecutive discharge and charge profiles.[19] During long-term (1h cycle) cyclability with a current density of 15 mA cm^{-2}, the CMO/N-rGO catalyst initially shows a discharge and charge overpotential of 0.51 and 0.33 V, which was increased to 0.53 and 0.35 V after eighth cycle, respectively. In contrast, Pt/C catalyst shows a discharge and charge overpotential increases quickly from 0.41 and 0.55 V to 0.61 and 1.04 V, respectively, after the eighth cycle. The round trip efficiency of CMO/N-rGO catalyst is 56% for the eighth cycle (58% for the first cycle) higher than that of precious Pt/C catalyst (39% for eighth cycle and 56% for first cycle). The specially blended CMO with N-rGO hybrid bifunctional catalyst showed a significant overpotential reduction and improved round trip efficiency over long-term cycles (Table 2). The excellent performance and durability over a high potential window of these hybrid electrocatalysts were attributed to the strong chemical coupling between CMO nanoparticles and the rGO support.[8] Moreover, we noticed that the hybrid catalysts showed significant oxygen electrochemistry with small overpotential for discharging and charging reactions for two electrode systems (pure oxygen and ambient air); they also showed comparable ORR -OER activity trends calculated from a three electrode system in alkaline medium (Table 1). The enhanced oxygen electrode activity of CMO/N-rGO catalyst can be attributed to the smaller and uniform dispersion of nanoparticles and strong coupling effect. All the XPS peaks of CMO/N-rGO shifted to higher binding energy compared with CMO-rGO corresponding to the strong interaction of metal oxide-rGO through nitrogen functional groups. This may be due to delocalization of donor−acceptor orbital interaction of metal with π-system of carbon framework in the rGO support through high affinity nitrogen groups. This results suggest that the strong interaction between CMO with N-rGO can provide a notable electrochemical activity with high stability.

Table 1. Summary of Charge and Discharge Potential Gap of Hybrid CMO-rGO and CMO/N-rGO with a Current Density of 20 mA cm^{-2} by Consuming Pure Oxygen and Air under Ambient Condition

	O_2 atmosphere						air atmosphere					
	1st cycle (V vs Zn)			100th cycle (V vs Zn)			1st cycle (V vs Zn)			100th cycle (V vs Zn)		
catalyst	charge potential	discharge potential	C−D potential gap	charge potential	discharge potential	C−D potential gap	charge potential	discharge potential	C−D potential gap	charge potential	discharge potential	C−D potential gap
CMO-rGO	1.90	1.19	0.71	1.99	0.98	1.01	2.09	1.14	0.95	2.13	1.03	1.1
CMO/N-rGO	1.78	1.08	0.70	1.90	1.04	0.86	1.95	1.25	0.70	2.06	1.13	0.93

dx.doi.org/10.1021/am5047476 | ACS Appl. Mater. Interfaces 2014, 6, 16545−16555

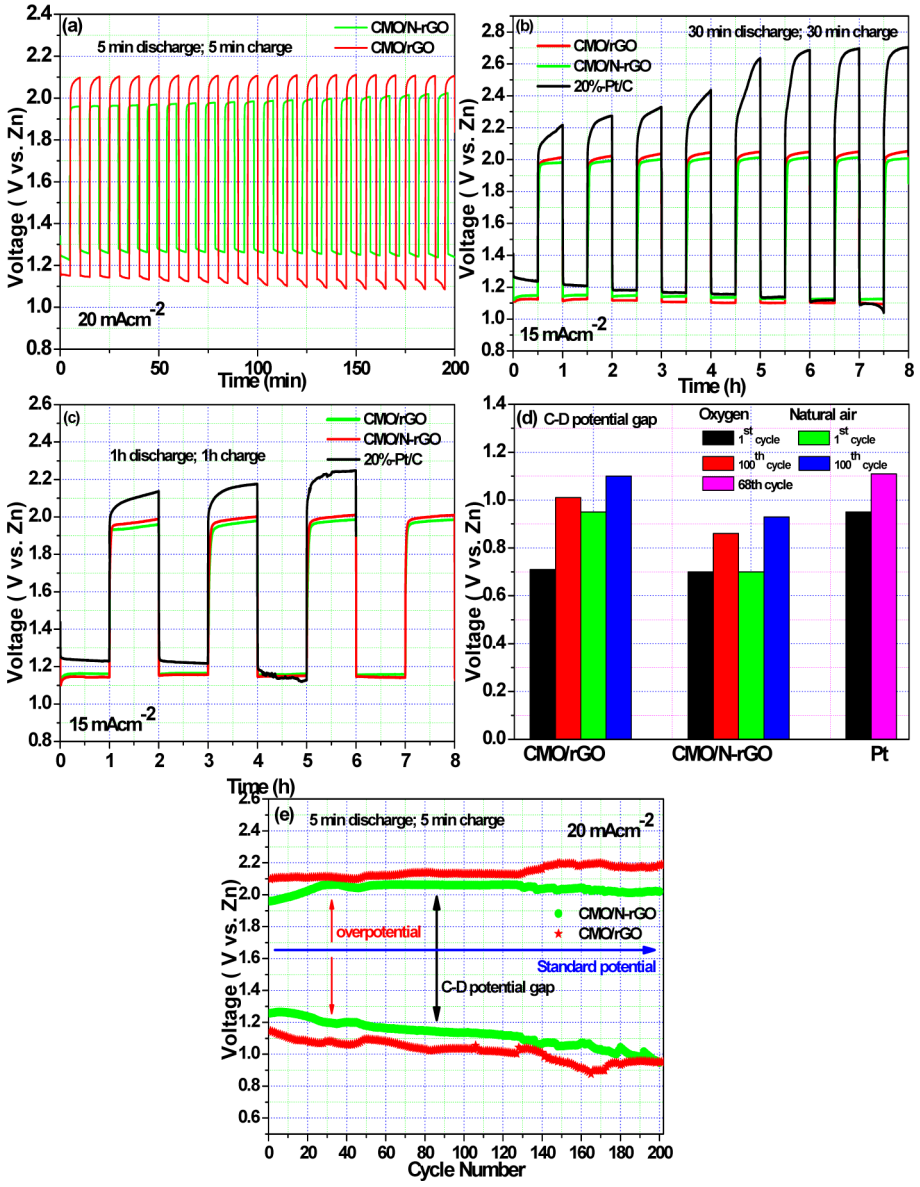

Figure 6. Galvanostatic pulse cycling of CMO/rGO and CMO/N-rGO hybrid under ambient air condition. (a) Cycling data at a current density 20 mA cm^{-2} in short interval (10 min per cycle) (b) Cycling data at a current density 15 mA cm^{-2} (1 h per cycle). (c) Cycling data at a current density 15 mA cm^{-2} in long interval (2 h per cycle) compared with Pt/C. (d) C−D potential gap comparison of Pt/C, CMO/rGO and CMO/N-rGO hybrid using pure oxygen and ambient air condition. (e) C−D potential gap vs cycle number for CMO/rGO and CMO/N-rGO hybrid consuming air under ambient condition.

Table 2. Overpotential and Round-Trip Efficiency Values of Pt/C, CMO/N-rGO, and CMO/rGO Catalysts during Long-Term (1 h cycle) Cyclability with a Current Density of 15 mA cm^{-2}

	1st cycle			8th cycle		
	overpotential (V)			overpotential (V)		
catalyst	discharge	charge	round-trip efficiency (%)	discharge	charge	round-trip efficiency (%)
Pt/C	0.41	0.55	56	0.61	1.04	39
CMO/N-rGO	0.51	0.33	58	0.53	0.35	56
CMO/rGO	0.53	0.35	56	0.55	0.39	54

We further examined the catalytic activity of the hybrid material with different current rates using the galvanodynamic method (Figure 7).[40] The hybrid materials show comparable discharging potential when compared with those of a noble metal catalyst Pt/C during the oxygen reduction reaction. On the other hand, during the charge process, the hybrid materials significantly outperformed the Pt/C materials. At higher potential, cyclic performance of Pt/C degrade enormously due to various side reactions like particle agglomeration, surface oxide formation and detachment of carbon from the support. But in the case of CMO/N-rGO hybrid, oxidation of N-rGO was not observed due to the strong chemical coupling between CMO and rGO. Further CMO nanoparticles with mixed valency afford donor−acceptor sites, which are highly active region for charging potential which suppressing the carbon corrosion. The hybrid catalyst CMO/N-rGO shows a small potential gap of 1.25 V, and CMO/rGO shows a potential gap of 1.65 V; these values are remarkable when compared with that of Pt/C: 1.94 V at 75 mA cm^{-2}.[14,17,41] The better stability

dx.doi.org/10.1021/am5047476 | ACS Appl. Mater. Interfaces 2014, 6, 16545−16555

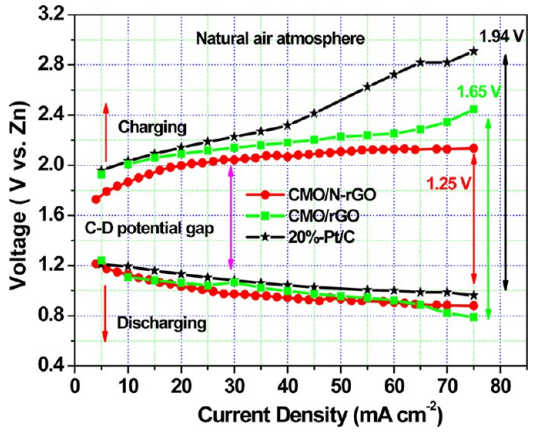

Figure 7. Galvanodynamic discharge and charge polarization curves of Pt/C, CMO/rGO, and CMO/N-rGO consuming air under ambient condition.

and activity of CMO with graphene over a long duration (over 200 cycles) and at higher current density are caused by strong the covalent coupling of CMO nanoparticles with the graphene layer; this coupling promotes a path for electron transfer on the electrode surface through the graphene network, which facilitates the charge−discharge reactions on the surface of the CMO nanoparticles.[12] Moreover, nitrogen doping in the graphene structure leads to the creation of many structural defects with positive effects of pyridinic and quaternary nitrogen; nitrogen doping also facilitates oxygen kinetics and fast transport of electrons.[29,30,33]

3.4. Structural and Morphological Stability. To understand the structural stability of hybrid cathode electrodes at various battery C−D cycles, XRD measurements were recorded after the 50th and 100th cycles; at these points we dismantled the air-breathing electrodes and compare along with the bare electrodes. For better comparison, a rietveld refinment process was carried out to check the various precipitates formed on the surface of the air cathode, with results as shown in Figure 8a, b. The XRD patterns of CMO/N-rGO and CMO/rGO after the 50th cycle of the electrodes, no appreciable change was observed when compared with as-prepared electrodes, except for slight changes in the relative intensities of the selected peaks as a result of slight formation of ZnO, which was amorphous in nature, with precipitation of carbonates (K_2CO_3) under ambient air. After the 100th charge−discharge cycle, the XRD patterns of both the hybrid electrodes show additional peaks with the crystallization of ZnO. When repeatedly battery was charged-discharged over 100 cycles, there was more precipitation of carbonates on the air electrode was observed under ambient air condition with alkaline electrolyte. Moreover, the discharge product $Zn(OH)_4^{2-}$ reached a saturation point in the alkaline electrolyte during discharge, causing zincate ions to decompose as white solid ZnO; these ions were eventually deposited on the surface of both anode and cathode and were not completely redeposited during given interval of charging.[23] Interestingly, no noticeable changes in the structure of the hybrid electrodes after the 50th or 100th cycles were found, which shows the structural stability of the hybrid materials toward zinc−air battery testing.[19]

Apart from the high structural stability, the morphology effect of the cycled electrodes was also tested and compared with that of bare electrodes, with results as shown in Figure 9a−f; we also include corresponding energy-dispersive X-ray spectroscopy

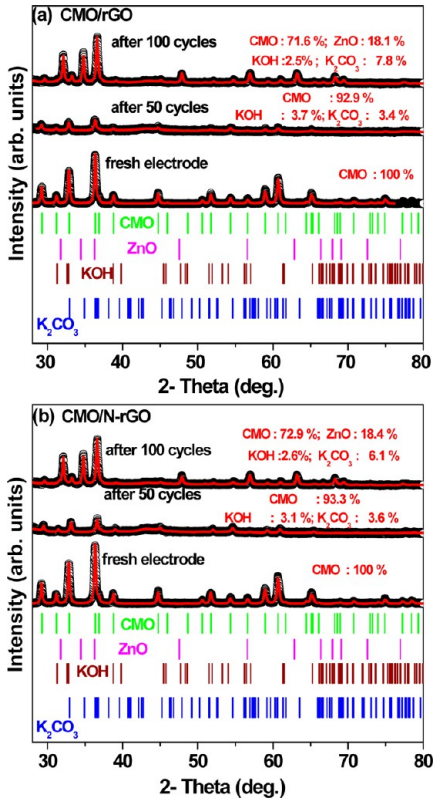

Figure 8. Rietveld refined XRD patterns of fresh and cycled (50th and 100th cycle) air electrodes: (a) CMO/rGO; (b) CMO/N-rGO. The symbols are experimental data and a continuous line is fitted data. The Miller indices (*h*, *k*, *l*) of different phase are shown.

(EDS) and elemental mapping results in Figure 10 (see Figure S3−S5 in the Supporting Information). Before cycling, the as-prepared hybrid electrode showed the uniform anchoring of CMO nanoparticles on the surface of the graphene layer, with a good distribution of Co, Mn, O, and N (Figures 9a, 10a). After the 50th cycle of the electrodes, slight formation of amorphous ZnO with precipitation of carbonates under ambient air, indicates the existence of K and Zn ions on the electrode. When the electrode was cycled after 100 cycles, $Zn(OH)_4^{2-}$ had reached its saturation point, and further decomposed and crystallized as white solid ZnO, which flooded more on the surface as confirmed by the XRD pattern (Figure 8). Furthermore, carbonate formation is more noticeable when the electrode is consuming air under ambient condition over 100 cycles, which was confirmed by the XRD and FTIR results (see Figures S6 and S7 in the Supporting Information).[21,22,42] Eventually, both hybrid materials retained chemical coupling between the nanoparticles and the graphene sheets[10] without any detachment of CMO nanoparticles from the graphene supports even though there was a pair of undesired reactions between positive and negative electrode materials with alkaline electrolyte over 100 cycles, with high oxidative charging potential.[19] Further, the porous nature of the hybrid material makes it optimal for both oxygen reduction during discharge and oxygen evolution during charging whereas the material Pt/C during oxygen gas evolution creates mechanical pressure, which causes a breakdown of the electrode when oxygen gas evolves at the electrode.[1]

Electrochemical impedance spectra is a useful technique to evaluate the issues affecting the electrical properties of the air

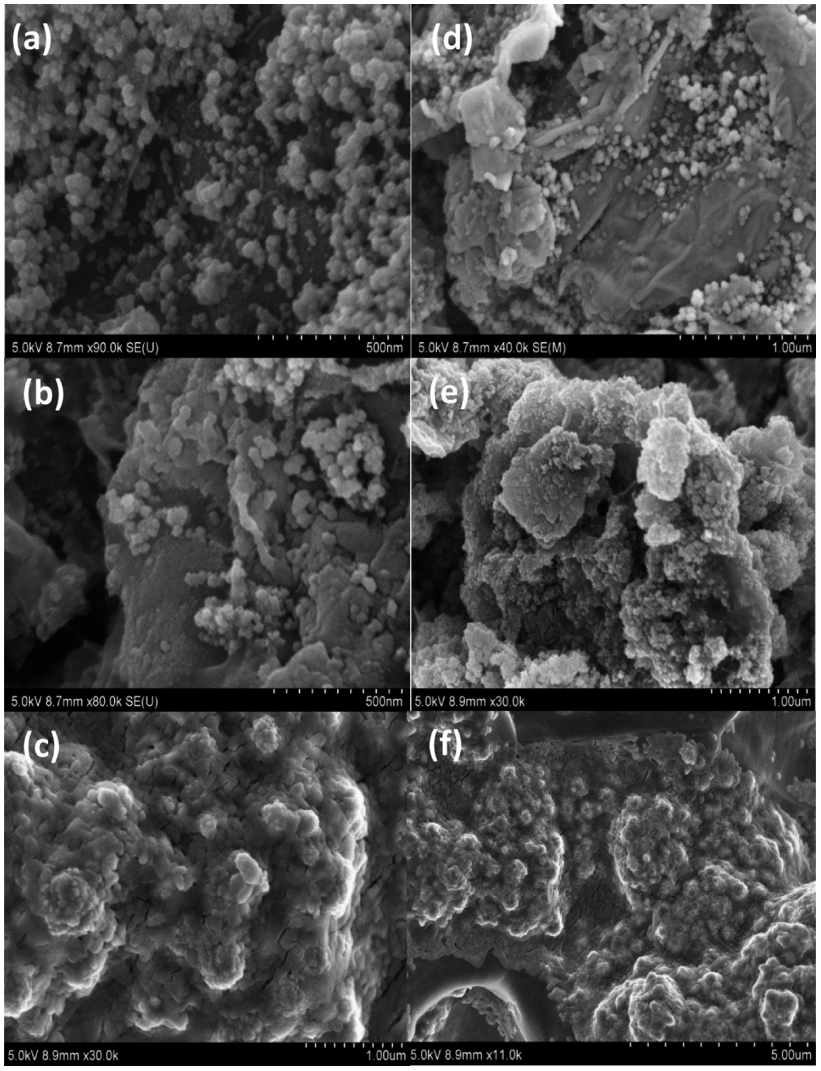

Figure 9. SEM images of fresh and cycled electrodes for CMO/N-rGO: (a) fresh, (b) after 50 cycles,(c) after 100 cycles. CMO/rGO: (d) fresh; (e) after 50 cycles; (f) after 100 cycles.

electrode under oxygen kinetics over repeated cycles.[43] The corresponding Nyquist plots (Z' vs $-Z''$) are shown in Figure 11. Each spectrum consists of two semicircles, one in the higher frequency region followed by one in the low frequency region. The impedance spectra were fitted using an equivalent circuit consisting of the resistance (electrolyte (R_s), solid−electrolyte interface (R_{int}), charge transfer (R_{ct}), and constant phase element ($Q_{(int+dl)}$) (interface (int) + double layer (dl)).[14,19] The extracted impedance parameters are listed in Table 3. The electrolyte resistance (R_s) remains almost constant, with only small change over a large number of cycles, due to the chemical and physical properties of the electrolyte. Both the solid−electrolyte interface resistance (R_{int}) and the charge transfer resistances (R_{ct}) increase significantly with increases in the cycle number due to the formation and precipitation of insulating ZnO on the electrolyte/electrode interface, along with carbonate formation. In the case of CMO/N-rGO, charge transfer resistance increases to 16 (Ω) after 100 cycles from 5 (Ω), whereas those values for CMO/rGO increased to 32 (Ω) from 13 (Ω); both of these should be much better when compared to the values of Pt/C, which increased to 21 (Ω) after 70 cycles from 3.6 (Ω). Further confirming its strong electrochemical coupling between nanoparticles and the graphene layer even after high charging potential, the CMO/N-rGO hybrid shows much lower resistance for both the solid-interface (R_{int}) and the charge transfer (R_{ct}) than does Pt/C. Finally, one can understand that the CMO/N-rGO catalyst shows a better plateau region, discharge time, and discharge capacity in a primary zinc−air battery, as well as higher activity and durability in a rechargeable zinc−air battery than CMO/rGO or the Pt/C catalyst; these excellent characteristics of the CMO/N-rGO catalyst can be shown to originate from its stable morphological and chemical structures (Figures 8−11). The reason behind the superior performance of CMO/N-rGO catalyst is that doping nitrogen in the graphene network allows for the uniform distribution of CMO particles on the graphene network, with various active sites; there is also the positive effect of pyridinic and quaternary nitrogen, which creates a synergic effect with this unique architecture.[44]

On the basis of the structural and morphological changes during electrochemical studies, it is pertinent to correlate the physical property of hybrid electrodes at various cycles. Interestingly, we found from the ex-situ XRD and SEM morphological analyses that during cycling there was no systematic change in the structure and morphology of hybrid catalyst rather than deposition of discharge products (ZnO) with

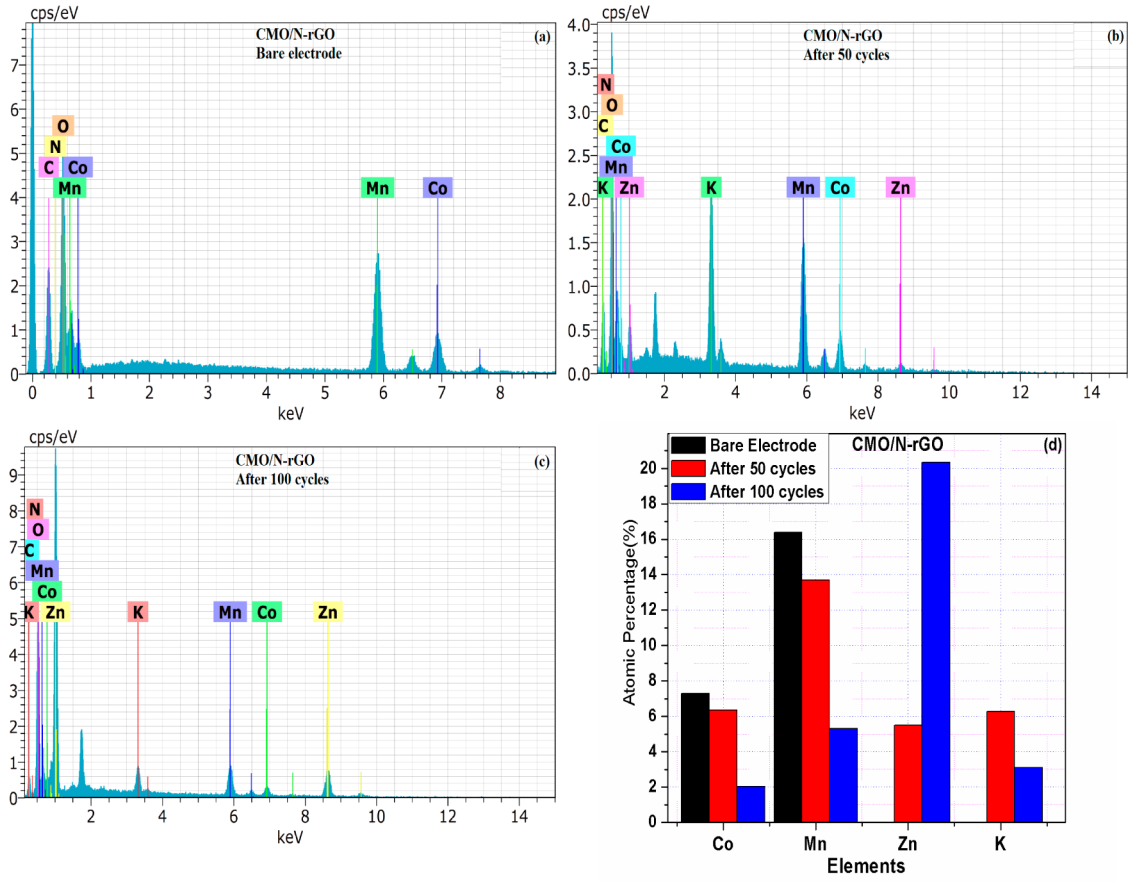

Figure 10. EDS spectrum of fresh and cycled CMO/N-rGO hybrid electrodes. (a) Fresh electrode; (b) after 50 cycles; (c) after 100 cycles; (d) atomic percentage of elements (Co, Mn, Zn, and K) over different cycled electrodes.

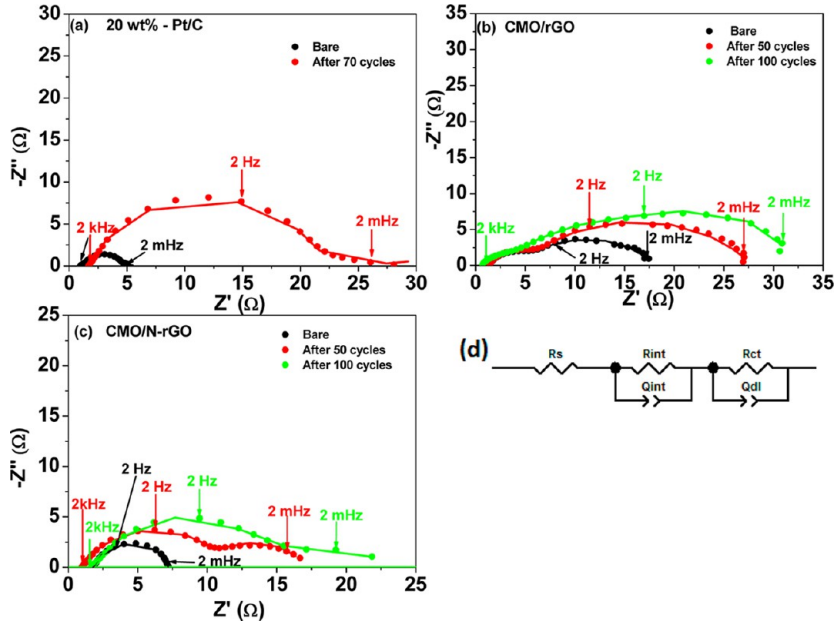

Figure 11. Nyquist plots (Z' vs $-Z''$) of zinc–air battery with air breathing cathode. (a) Pt/C, (b) CMO/rGO, (c) CMO/N-rGO consuming air under ambient condition. (d) Corresponding equivalent electrical circuit. Impedance was taken at DC potential of 0.8 V with an AC signal amplitude of 10 mV by variable frequency range from 10 kHz to 10 mHz.

carbonate formation (K_2CO_3) on the surface under ambient condition. The nitrogen-doped graphene oxide surface provides a robust support for the electroactive CMO nanoparticles anchoring through the nitrogen-doped carbon and further improves the electrical conductivity, but also has the positive effect of high specific surface area with high porosity that favors

dx.doi.org/10.1021/am5047476 | ACS Appl. Mater. Interfaces 2014, 6, 16545–16555

Table 3. Impedance Parameters Derived from Nyquist Plots of Pt/C, CMO/N-rGO, and CMO/rGO Catalyst at Various Cycles

impedance parameters	cycle no.	CMO-rGO	CMO/N-rGO	Pt/C
R_s (Ω)	bare	1.387	1.456	1.045
	50th	1.412	1.145	1.755
	100th	1.019	1.671	(70th)
R_{int} (Ω)	bare	3.317	0.959	0.196
	50th	3.56	3.083	8.289
	100th	4.913	4.741	(70th)
R_{ct} (Ω)	bare	13.39	5.508	3.651
	50th	22.92	15.65	21.11
	100th	32.43	16.04	(70th)
Q_{int} (F)	bare	0.0004	0.0001	0.00045
	50th	0.0037	0.0014	0.068
	100th	0.05	0.012	(70th)
α	bare	0.82	0.83	0.87
	50th	0.77	0.75	0.65
	100th	0.71	0.69	(70th)
Q_{dl} (F)	bare	0.0953	0.02	0.002
	50th	0.0724	0.011	0.934
	100th	0.051	0.045	(70th)
α	bare	0.71	0.75	0.77
	50th	0.69	0.70	0.68
	100th	0.61	0.65	(70th)

the oxygen transport without any mechanical pressure created during oxygen gas evolution at charging. The extended cycling (1 h cycle) of CMO/N-rGO hybrid electrodes show comparable performance with small increment in overpotential can be observed on both the charge and discharge segments caused by undesirable carbonate formation (K_2CO_3) and crystallization of ZnO on the cathode surface (see Figure S8 in the Supporting Information). The stronger electronegativity of doped-nitrogen and the lone pair of electrons on nitrogen facilitates the connection between electroactive CMO nanoparticles to the graphene and electrolyte and reduce the particle size from agglomerating and protecting active materials from mechanical degradation during different cycles. The strong hybridization CMO particles on rGO through nitrogen functional groups greatly reducing the undesired decomposition and side reaction of carbon based support which was often promoted simultaneously at charging condition. During long-term cycling the concentration of the zincate ion surpasses the maximum limit of solubility, thereby causing dehydration and precipitation of ZnO which passivates the zincate formation from the anode led to the cell failure (see Figure S6 in the Supporting Information). A systematic post-mortem analysis further confirms that the pair of undesired parasitic reactions between positive (carbonate formation under ambient condition) and negative electrode (hydrogen evolution) with the alkaline electrolyte that consumes air under ambient condition is mainly responsible for the observed performance deterioration. From the correlation, we have reason to expect the high catalytic activity with a small degradation extended over a longer life span.

5. CONCLUSIONS

In summary, we have prepared a nitrogen doped/undoped thermally reduced graphene oxide support decorated chemically with CMO nanoparticles using a one step hydrothermal method. Under ambient air condition, the primary and rechargeable zinc−air battery using the CMO/N-rGO hybrid bifunctional air electrode with strong alkaline electrolyte shows outstanding discharge and charge performance while maintaining good stability when operated over 200 cycles. The unique structural, morphological, and electrocatalytic properties of the CMO/N-rGO hybrid, compared with those of the commercial Pt/C catalyst, make this hybrid material a promising candidate for zinc−air battery applications.

■ ASSOCIATED CONTENT

Supporting Information

Additional characterization data of photographic image of cycled electrodes (anode and cathode) XPS, SEM-elemental mapping, point EDS, FTIR spectrum, and extended galvanostatic pulse cycling of cycled electrodes for hybrid and XRD pattern of the cycled zinc anode. This material is available free of charge via the Internet at http://pubs.acs.org.

■ AUTHOR INFORMATION

Corresponding Author

*E-mail: sangarajus@dgist.ac.kr. Tel.: +82 53 785 6413; Fax: +82-53-785-6409.

Notes

The authors declare no competing financial interest.

■ ACKNOWLEDGMENTS

This work was supported by the DGIST R&D Program (14-BD-01) of the Ministry of Education, Science and Technology of Korea.

■ REFERENCES

(1) Rahman, M. A.; Wang, X.; Wen, C. High Energy Density Metal-Air Batteries: A Review. *J. Electrochem. Soc.* **2013**, *160*, A1759−A1771.

(2) Toussaint, G.; Stevens, P.; Akrour, L.; Rouget, R.; Fourgeot, F. Development of a Rechargeable Zinc-Air Battery. *ECS Trans.* **2010**, *28*, 25−34.

(3) Gittleson, F. S.; Sekol, R. C.; Doubek, G.; Linardi, M.; Taylor, A. D. Catalyst and Electrolyte Synergy in Li-O_2 Batteries. *Phys. Chem. Chem. Phys.* **2014**, *16*, 3230−3237.

(4) Girishkumar, G.; McCloskey, B.; Luntz, A. C.; Swanson, S.; Wilcke, W. Lithium−Air Battery: Promise and Challenges. *J. Phys. Chem. Lett.* **2010**, *1*, 2193−2203.

(5) Ryu, W.-H.; Yoon, T.-H.; Song, S. H.; Jeon, S.; Park, Y.-J.; Kim, I.-D. Bifunctional Composite Catalysts Using Co_3O_4 Nanofibers Immobilized on Nonoxidized Graphene Nanoflakes for High-Capacity and Long-Cycle Li-O_2 Batteries. *Nano Lett.* **2013**, *13*, 4190−4197.

(6) Du, G.; Liu, X.; Zong, Y.; Hor, T. S. A.; Yu, A.; Liu, Z. Co_3O_4 Nanoparticle-Modified MnO_2 Nanotube Bifunctional Oxygen Cathode Catalysts for Rechargeable Zinc-Air Batteries. *Nanoscale* **2013**, *5*, 4657−4661.

(7) Lee, J.-S.; Park, G. S.; Lee, H. I.; Kim, S. T.; Cao, R.; Liu, M.; Cho, J. Ketjenblack Carbon Supported Amorphous Manganese Oxides Nanowires as Highly Efficient Electrocatalyst for Oxygen Reduction Reaction in Alkaline Solutions. *Nano Lett.* **2011**, *11*, 5362−5366.

(8) Li, Y.; Gong, M.; Liang, Y.; Feng, J.; Kim, J.-E.; Wang, H.; Hong, G.; Zhang, B.; Dai, H. Advanced Zinc-Air Batteries Based on High-Performance Hybrid Electrocatalysts. *Nat. Commun.* **2013**, *4*, 1805.

(9) Cao, R.; Lee, J.; Liu, M.; Cho, J. Recent Progress in Non-Precious Catalysts for Metal-Air Batteries. *Adv. Energy Mater.* **2012**, *2*, 816−829.

(10) Prabu, M.; Ramakrishnan, P.; Shanmugam, S. $CoMn_2O_4$ Nanoparticles Anchored on Nitrogen-Doped Graphene Nanosheets as Bifunctional Electrocatalyst for Rechargeable Zinc−air Battery. *Electrochem. commun.* **2014**, *41*, 59−63.

(11) Prabu, M.; Ketpang, K.; Shanmugam, S. Hierarchical Nanostructured $NiCo_2O_4$ as an Efficient Bifunctional Non-Precious Metal

Catalyst for Rechargeable Zinc-Air Batteries. *Nanoscale* **2014**, *6*, 3173−3181.
(12) Bian, W.; Yang, Z.; Strasser, P.; Yang, R. A $CoFe_2O_4$/ Graphene Nanohybrid as an Efficient Bi-Functional Electrocatalyst for Oxygen Reduction and Oxygen Evolution. *J. Power Sources* **2014**, *250*, 196−203.
(13) Chen, Z.; Choi, J.; Wang, H.; Li, H.; Chen, Z. Highly Durable and Active Non-Precious Air Cathode Catalyst for Zinc Air Battery. *J. Power Sources* **2011**, *196*, 3673−3677.
(14) Chen, Z.; Yu, A.; Higgins, D.; Li, H.; Wang, H.; Chen, Z. Highly Active and Durable Core-Corona Structured Bifunctional Catalyst for Rechargeable Metal-Air Battery Application. *Nano Lett.* **2012**, *12*, 1946−1952.
(15) Lee, J.-S.; Lee, T.; Song, H.-K.; Cho, J.; Kim, B.-S. Ionic Liquid Modified Graphene Nanosheets Anchoring Manganese Oxide Nanoparticles as Efficient Electrocatalysts for Zn−air Batteries. *Energy Environ. Sci.* **2011**, *4*, 4148.
(16) Wang, H.; Yang, Y.; Liang, Y.; Zheng, G.; Li, Y.; Cui, Y.; Dai, H. Rechargeable $Li-O_2$ Batteries with a Covalently Coupled $MnCo_2O_4$−Graphene Hybrid as an Oxygen Cathode Catalyst. *Energy Environ. Sci.* **2012**, *5*, 7931.
(17) Jung, K.-N.; Jung, J.-H.; Im, W. B.; Yoon, S.; Shin, K.-H.; Lee, J.-W. Doped Lanthanum Nickelates with a Layered Perovskite Structure as Bifunctional Cathode Catalysts for Rechargeable Metal-Air Batteries. *ACS Appl. Mater. Interfaces* **2013**, *5*, 9902−9907.
(18) Zhu, S.; Chen, Z.; Li, B.; Higgins, D.; Wang, H.; Li, H.; Chen, Z. Nitrogen-Doped Carbon Nanotubes as Air Cathode Catalysts in Zinc-Air Battery. *Electrochim. Acta* **2011**, *56*, 5080−5084.
(19) Lee, D. U.; Choi, J.-Y.; Feng, K.; Park, H. W.; Chen, Z. Advanced Extremely Durable 3D Bifunctional Air Electrodes for Rechargeable Zinc-Air Batteries. *Adv. Energy Mater.* **2014**, *4*, 1−5.
(20) Xu, L.; Ma, J.; Li, B.; Kang, F. A Novel Air Electrode Design: A Key to High Rate Capability and Long Life Span. *J. Power Sources* **2014**, *255*, 187−196.
(21) Bhatt, A.; Kao, P.; Best, A.; Hollenkamp, A. Li-Air and Li-S Batteries: Understanding the Morphological Changes of Lithium Surfaces during Cycling at a Range of Current Densities in an Ionic Liquid Electrolyte. *ECS Trans.* **2013**, *50*, 383−401.
(22) Shaigan, N.; Qu, W.; Takeda, T. Morphology Control of Electrodeposited Zinc from Alkaline Zincate Solutions for Rechargeable Zinc Air Batteries. *ECS Trans.* **2010**, *28*, 35−44.
(23) Parker, J. F.; Chervin, C. N.; Nelson, E. S.; Rolison, D. R.; Long, J. W. Wiring Zinc in Three Dimensions Re-Writes Battery Performance—Dendrite-Free Cycling. *Energy Environ. Sci.* **2014**, *7*, 1117.
(24) Cherian, C. T.; Zheng, M.; Reddy, M. V.; Chowdari, B. V. R.; Sow, C. H. Zn_2SnO_4 Nanowires versus Nanoplates: Electrochemical Performance and Morphological Evolution during Li-Cycling. *ACS Appl. Mater. Interfaces* **2013**, *5*, 6054−6060.
(25) Han, X.; Hu, Y.; Yang, J.; Cheng, F.; Chen, J. Porous Perovskite $CaMnO_3$ as an Electrocatalyst for Rechargeable $Li-O_2$ Batteries. *Chem. Commun.* **2014**, *50*, 1497−1499.
(26) Zhang, T.; Zhou, H. A Reversible Long-Life Lithium-Air Battery in Ambient Air. *Nat. Commun.* **2013**, *4*, 1817.
(27) Shen, Y.; Sun, D.; Yu, L.; Zhang, W.; Shang, Y.; Tang, H.; Wu, J.; Cao, A.; Huang, Y. A High-Capacity Lithium−air Battery with Pd Modified Carbon Nanotube Sponge Cathode Working in Regular Air. *Carbon* **2013**, *62*, 288−295.
(28) Hummers, W. S.; Offeman, R. E. Preparation of Graphitic Oxide. *J. Am. Chem. Soc.* **1958**, *80*, 1339−1339.
(29) Liang, Y.; Wang, H.; Zhou, J.; Li, Y.; Wang, J.; Regier, T.; Dai, H. Covalent Hybrid of Spinel Manganese-Cobalt Oxide and Graphene as Advanced Oxygen Reduction Electrocatalysts. *J. Am. Chem. Soc.* **2012**, *134*, 3517−3523.
(30) Liang, Y.; Li, Y.; Wang, H.; Zhou, J.; Wang, J.; Regier, T.; Dai, H. Co_3O_4 Nanocrystals on Graphene as a Synergistic Catalyst for Oxygen Reduction Reaction. *Nat. Mater.* **2011**, *10*, 780−786.
(31) Wang, H.-W.; Hu, Z.-A.; Chang, Y.-Q.; Chen, Y.-L.; Wu, H.-Y.; Zhang, Z.-Y.; Yang, Y.-Y. Design and Synthesis of $NiCo_2O_4$−reduced Graphene Oxide Composites for High Performance Supercapacitors. *J. Mater. Chem.* **2011**, *21*, 10504.
(32) Chen, S.; Zhu, J.; Wu, X.; Han, Q.; Wang, X. Graphene Oxide-MnO_2 Nanocomposites for Supercapacitors. *ACS Nano* **2010**, *4*, 2822−2830.
(33) Liu, Q.; Jin, J.; Zhang, J. $NiCo_2S_4$@Graphene as a Bifunctional Electrocatalyst for Oxygen Reduction and Evolution Reactions. *ACS Appl. Mater. Interfaces* **2013**, *5*, 5002−5008.
(34) Wang, L.; Zhao, X.; Lu, Y.; Xu, M.; Zhang, D.; Ruoff, R. S.; Stevenson, K. J.; Goodenough, J. B. $CoMn_2O_4$ Spinel Nanoparticles Grown on Graphene as Bifunctional Catalyst for Lithium-Air Batteries. *J. Electrochem. Soc.* **2011**, *158*, A1379.
(35) Bi, E.; Chen, H.; Yang, X.; Peng, W.; Grätzel, M.; Han, L. A Quasi Core−shell Nitrogen-Doped Graphene/cobalt Sulfide Conductive Catalyst for Highly Efficient Dye-Sensitized Solar Cells. *Energy Environ. Sci.* **2014**, *7*, 2637.
(36) Nam, G.; Park, J.; Kim, S. T.; Shin, D.; Park, N.; Kim, Y.; Lee, J.-S.; Cho, J. Metal-Free Ketjenblack Incorporated Nitrogen-Doped Carbon Sheets Derived from Gelatin as Oxygen Reduction Catalysts. *Nano Lett.* **2014**, *14*, 1870−1876.
(37) Xie, Y.; Li, H.; Tang, C.; Li, S.; Li, J.; Lv, Y.; Wei, X.; Song, Y. A High-Performance Electrocatalyst for Oxygen Reduction Based on Reduced Graphene Oxide Modified with Oxide Nanoparticles, Nitrogen Dopants, and Possible Metal-N-C Sites. *J. Mater. Chem. A* **2014**, *2*, 1631.
(38) Li, Y.; Dai, H. Recent Advances in Zinc-Air Batteries. *Chem. Soc. Rev.* **2014**, *43*, 5257−5275.
(39) Wang, Z.; Xu, D.; Xu, J.; Zhang, X. Oxygen Electrocatalysts in Metal−air Batteries: From Aqueous to Nonaqueous Electrolytes. *Chem. Soc. Rev.* **2014**, DOI: 10.1039/C3CS60248F.
(40) Kubo, D.; Tadanaga, K.; Hayashi, A.; Tatsumisago, M. Multifunctional Inorganic Electrode Materials for High-Performance Rechargeable Metal−air Batteries. *J. Mater. Chem. A* **2013**, *1*, 6804.
(41) Chen, Z.; Yu, A.; Ahmed, R.; Wang, H.; Li, H.; Chen, Z. Manganese Dioxide Nanotube and Nitrogen-Doped Carbon Nanotube Based Composite Bifunctional Catalyst for Rechargeable Zinc-Air Battery. *Electrochim. Acta* **2012**, *69*, 295−300.
(42) Wittmaier, D.; Danner, T.; Wagner, N.; Friedrich, K. A. Screening and Further Investigations on Promising Bi-Functional Catalysts for Metal−air Batteries with an Aqueous Alkaline Electrolyte. *J. Appl. Electrochem.* **2013**, *44*, 73−85.
(43) Zhuang, S.; Zhang, H.; Liu, S.; Tu, F. Optimized Perovskite Electrocatalyst for Bifunctional Air Electrode by Impedance Spectroscopy Analysis. *Int. J. Electrochem.Sci.* **2014**, *9*, 1690−1701.
(44) Duan, J.; Zheng, Y.; Chen, S.; Tang, Y.; Jaroniec, M.; Qiao, S. Mesoporous Hybrid Material Composed of Mn_3O_4 Nanoparticles on Nitrogen-Doped Graphene for Highly Efficient Oxygen Reduction Reaction. *Chem. Commun.* **2013**, *49*, 7705−7707.